Nitrogen mass transfer and surface layer formation during the active screen plasma nitriding of austenitic stainless steels

Lin, Kaijie; Li, Xiaoying; Dong, Hanshan; Guo, Ping; Gu, Dongdong

DOI:
10.1016/j.vacuum.2017.11.022

Document Version
Peer reviewed version

Citation for published version (Harvard):
Lin, K, Li, X, Dong, H, Guo, P & Gu, D 2018, 'Nitrogen mass transfer and surface layer formation during the active screen plasma nitriding of austenitic stainless steels', *Vacuum*, vol. 148, pp. 224-229. https://doi.org/10.1016/j.vacuum.2017.11.022

Accepted Manuscript

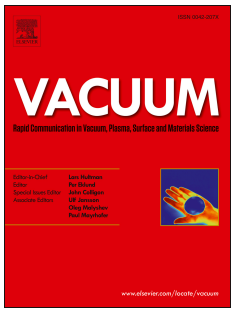

Nitrogen mass transfer and surface layer formation during the active screen plasma nitriding of austenitic stainless steels

Kaijie Lin, Xiaoying Li, Hanshan Dong, Ping Guo, Dongdong Gu

PII: S0042-207X(17)31175-2

DOI: 10.1016/j.vacuum.2017.11.022

Reference: VAC 7691

To appear in: *Vacuum*

Received Date: 30 August 2017

Revised Date: 7 November 2017

Accepted Date: 13 November 2017

Please cite this article as: Lin K, Li X, Dong H, Guo P, Gu D, Nitrogen mass transfer and surface layer formation during the active screen plasma nitriding of austenitic stainless steels, *Vacuum* (2017), doi: 10.1016/j.vacuum.2017.11.022.

Nitrogen mass transfer and surface layer formation during the active screen plasma nitriding of austenitic stainless steels

Kaijie Lin [a,b,c], Xiaoying Li [c], Hanshan Dong [c], Ping Guo [d], Dongdong Gu[a,b,*]

[a]*College of Materials Science and Technology, Nanjing University of Aeronautics and Astronautics, 29 Yudao Street, Nanjing210016, People's Republic of China*

[b] *Institute of Additive Manufacturing (3D Printing), Nanjing University of Aeronautics and Astronautics, 29 Yudao Street, Nanjing210016, People's Republic of China*

[c]*School of Metallurgy and Materials, The University of Birmingham, Edgbaston, Birmingham B15 2TT, UK*

[d] *Nanjing Boiler and Pressure Vessel Inspection Institute, 3 Jialingjiang East Road, Nanjing 210002, People's Republic of China*

Abstract:

Active screen plasma nitriding (ASPN), a novel surface modification process, has been widely applied to improve various surface properties of austenitic stainless steels, such as wear resistance, electrical conductivity and corrosion resistance. All the improvement of surface properties attributes to the formation of a unique phase under low nitriding temperature, called S-phase. A "sputter – deposit – decompose – diffusion model" has been established to explain the formation of S-phase, however, the mechanism of nitrogen mass transfer to the substrate during ASPN still remains controversial. By comprehensively comparing the surface responds of three different surfaces (bare 316L stainless steel surface, Au-coated 316L stainless steel surface and Si wafer surface) during ASPN treatments, this paper provides the direct evidence and clarifies the mechanism of nitrogen mass transfer between the deposition layer and the substrate during ASPN treatment.

Keywords: Active screen plasma nitriding; Nitrogen mass transfer; Surface structure; 316L stainless steel

*Corresponding author: dongdonggu@nuaa.edu.cn

1. Introduction

Active screen plasma nitriding (ASPN) technology has received considerable studies since it was invented by J. Geoges in the early 2000s. [1] This novel surface plasma technology offers many advantages over the conventional direct current plasma method, such as better surface quality and layer uniformity [2], and has been applied in the field of medical devices [3–5], orthopaedic devices [6–8] and hydrogen fuel cells [9–14].

The mechanism of active screen plasma technology has also been extensively investigated. Inspired by the mechanism of direct current plasma nitriding (DCPN), Li et al. [15] proposed a "sputtering and recondensation model" to explain the ASPN process. In this model, the mass transfer of nitrogen was contributed by the sputtering of iron nitride from the cathodic metal screen and depositing onto the sample surface. Based on Li's model, Zhao et al. [16,17] developed a more detailed model, stating that ASPN was a multi-stages process, including:1) particles sputtered from the screen then adsorbing active nitrogen species in the plasma; 2) nitrogen-rich particles (Fe_xN) deposited on the sample surface; 3) nitrogen releasing from the particles and diffusing into the substrate. This model was supported by the studies of Corujeira Gallo and Dong [18], who found the present of XRD peaks of deposited materials (FeN and Fe_xN) on the surface of treated samples. However, Hubbard and co-workers claimed in their researches [19,20] that there was no direct evidence for nitrogen mass transfer between the deposition layer and the substrate. They believed that a flux of energetic nitrogen species generated by the active screen bombarded the samples and transferred the nitrogen to the surface of samples.

In this study, a special designed experiment was conducted to provide the direct evidence of mass transfer between the deposition layer and the substrate. Bare 316L stainless steel surfaces, Au-coated 316L stainless steel surfaces and Si wafer surfaces were treated simultaneously by ASPN. Au is noble and do not react with nitrogen [21], therefore Au coating was selected as barrier layer to retard the possible diffusion of nitrogen into the 316L stainless steel substrate. It is known that the solid solubility of nitrogen in Si wafer is very low [22]and hence the as-deposition layer could be retained on the surface of Si wafer. By comparing the responds of different surfaces under the same ASPN setting and investigating the microstructure of layers on different surfaces, the nitrogen mass transfer in ASPN was expected to be revealed.

2. Material and methods

Coupon samples of 316 stainless steel (SS) were cut from a hot rolled bar using SiC cutting wheel in the thickness of 6mm. The surfaces of samples were wet ground from 240 grit up to 1200 grit, followed by polishing with diamond paste from 6μm down to 1μm. Prior to the ASPN treatment, the polished surface of 316 SS sample was partly deposited with Au coating in vacuum gold-coater for 3min (the thickness of Au coating was about 350nm), the rest part of the surface was left bare. During the ASPN treatments, Si wafers were placed on the surface of 316 SS samples and treated simultaneously. The detail of the ASPN treatments can be found in previous publications[11][14]. The main power was applied on the big active screen to generate plasma and control temperature. The bias was applied on the small active screen via the worktable. The samples alongside with the Si wafer on its surface were placed on an insulated table inside the small active screen and hence stayed at a floating potential

during treatment (Figure 1). The temperature was measured by a thermocouple, which was placed on the insulated table and next to the treated samples. The ASPN treatment parameters, optimized in preliminary research, are listed as follow: temperature 450℃, applied bias 5% of the main power supply of 15 kVA , pressure 0.75mbar and gas mixture 25%N_2+75%H_2. The treatment durations were set as 15h, 20h and 30h. Before the ASPN treatment, the small 316L stainless steel screen used in this study was ASPN treated (with the same parameters listed above) for 10h to remove any contamination and oxide layer on its surface. The surface and cross-sectional morphology of samples after ASPN treatments were observed by scanning electron microscopy (SEM, Jeol 7000) and the surface composition was measured by energy disperse spectroscopy (EDS, Oxford Instrument Inca). The element depth profiles were obtained by glow discharge optical emission spectroscopy (GDOES, Leco GDS-750).

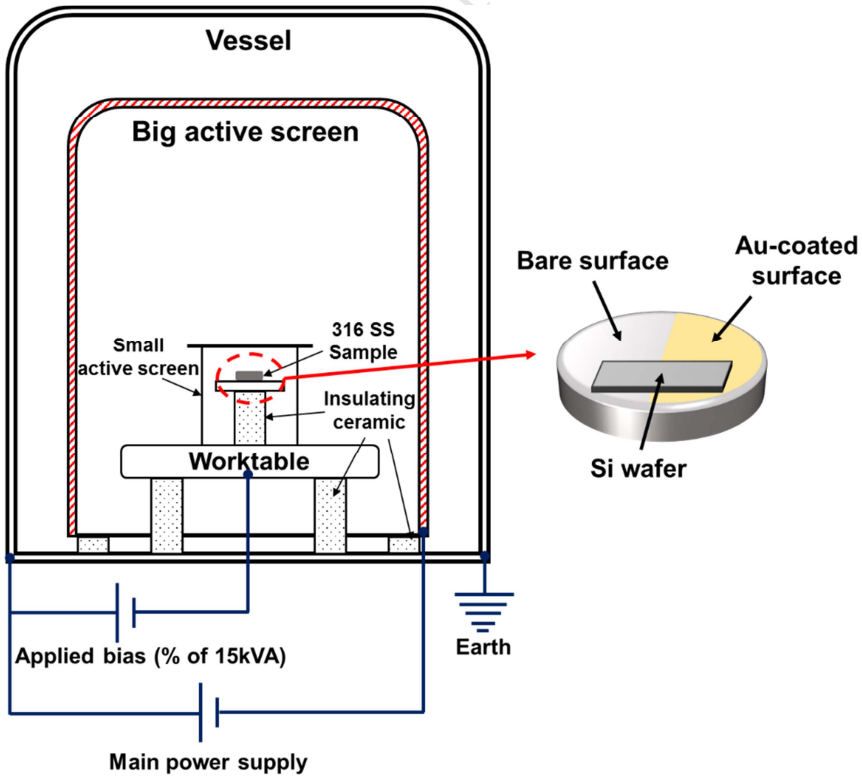

Figure 1 Schematic diagram of active screen plasma nitriding treatments

3. Results and discussion

The surface SEM images of bare surfaces (15h, 20h and 30h), Au-coated surfaces (Au-15h, Au-20h and Au-30h) and Si wafer surfaces (Si-15h, Si-20h and Si-30h) after different duration treatments are shown in Figure 2. The low magnification images are shown as inlet for bare surfaces and Au-coated surfaces. Under low magnification, the surface morphology of ASPN treated Si wafer is very similar to that of the ASPN treated Au-coated surface, and thus the low magnification images of Si wafers are not presented. From the low magnification images of the ASPN bare surfaces, surface relief, a typical surface respond of the formation of S-phase[12][23] [24], can be clearly observed. The formation of surface relief is attributed to the anisotropic diffusion of nitrogen in grains with different crystallographic orientations, leading to different expansion of neighbouring grains [25]. On the other hand, no evidence of surface relief can be observed from the Au-coated surfaces and Si wafer surfaces, even after 30 h treatment. From the high magnification SEM images, it can be clearly observed that each surface is covered by a layer of nano-size particles, which exhibit polyhedral feature. From the XRD pattern of the Si-30h sample (Figure 2 (j)), the XRD peaks of Si (PDF#27-1402), SiO_2 (PDF#51-1378), Fe_4N (PDF#83-0875), Fe and FeN [18] could be found. Therefore, most of these particles should be nitrides. Based on previous literatures [15,16], these particles are sputtered from the active screen and deposit onto the surface during treatment. Regardless of different surfaces, the size of particle and density of layer increase with the increase of treatment duration. Under the same treatment duration, the size of particles on three surfaces is similar. However, for 15 h and 20 h ASPN treated surfaces, the deposited particles on the bare surfaces are more

tightly packed (less pores among particles) than that deposited on the Au-coated surfaces and Si wafer surfaces. When treated for 30h, the surface morphology of the three different surfaces is almost identical.

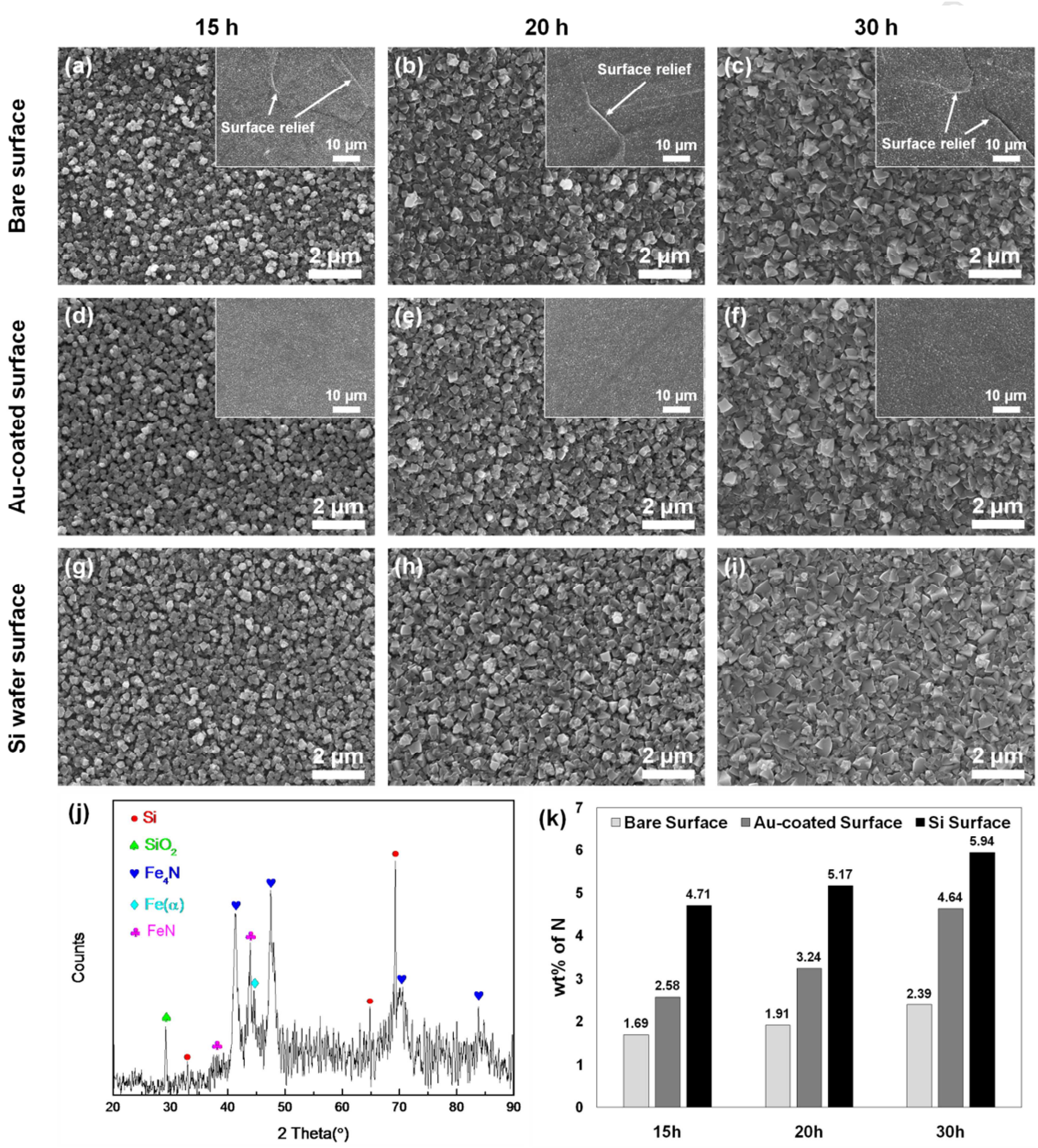

Figure 2 The surface morphology SEM images of different surfaces: (a) Bare-15h, (b) Bare-20h, (c) Bare-30h, (d) Au-15h, (e) Au-20h, (f) Au-30h,(g) Si-15h, (h) Si-20h, (i) Si-30h; (j) the XRD patterns of Si-30h sample; (k) the nitrogen contents of bare surfaces, Au-coated surfaces and Si surfaces after different treatment durations

The nitrogen content of different surfaces was measured by EDS and the results are charted in Figure 2 (k). Take the 15h group for instance, the content of nitrogen on the ASPN Si wafer surfaces is the highest, followed by the ASPN Au-coated surface and the ASPN bare surfaces have the lowest nitrogen content. The same trend is witnessed for other two treatment durations. In addition, regardless of different surfaces, the nitrogen content increases with the increase of treatment duration.

The low magnification cross-sectional SEM images of bare surfaces and Au-coated surfaces after different duration ASPN treatment are shown in Figure 3. No S-phase layer can be found from the Si surfaces, therefore their low magnification cross-sectional SEM images are not presented. In Figure 3 (a-f), featureless layers (marked by white arrows) can be found from all bare surfaces and Au-coated surfaces and the thickness of the layer was measured and present in Figure 3 (g). These layers are the so-called “S-phase layer”, which is a metastable, precipitate free, interstitial supersaturated “expanded austenite” [26]. It can be seen that, for both bare surface and Au-coated surface, the thickness of S-phase increases with treatment duration. Under the same treatment duration, the layer thickness of bare surface is significantly thicker than that of the Au-coated surface. The S-phase thickness of ASPN bare surface under 15h, 20h and 30h is 18 times, 9.7 times and 6.6 times thicker than that of the corresponding ASPN Au-coated surfaces, respectively. Besides the huge difference in layer thickness, the nitrogen content of S-phase is also significantly different. From the GDS nitrogen profiles shown in Figure 3 (h), the nitrogen depth profiles of bare surfaces are greatly higher than that of the Au-coated surfaces.

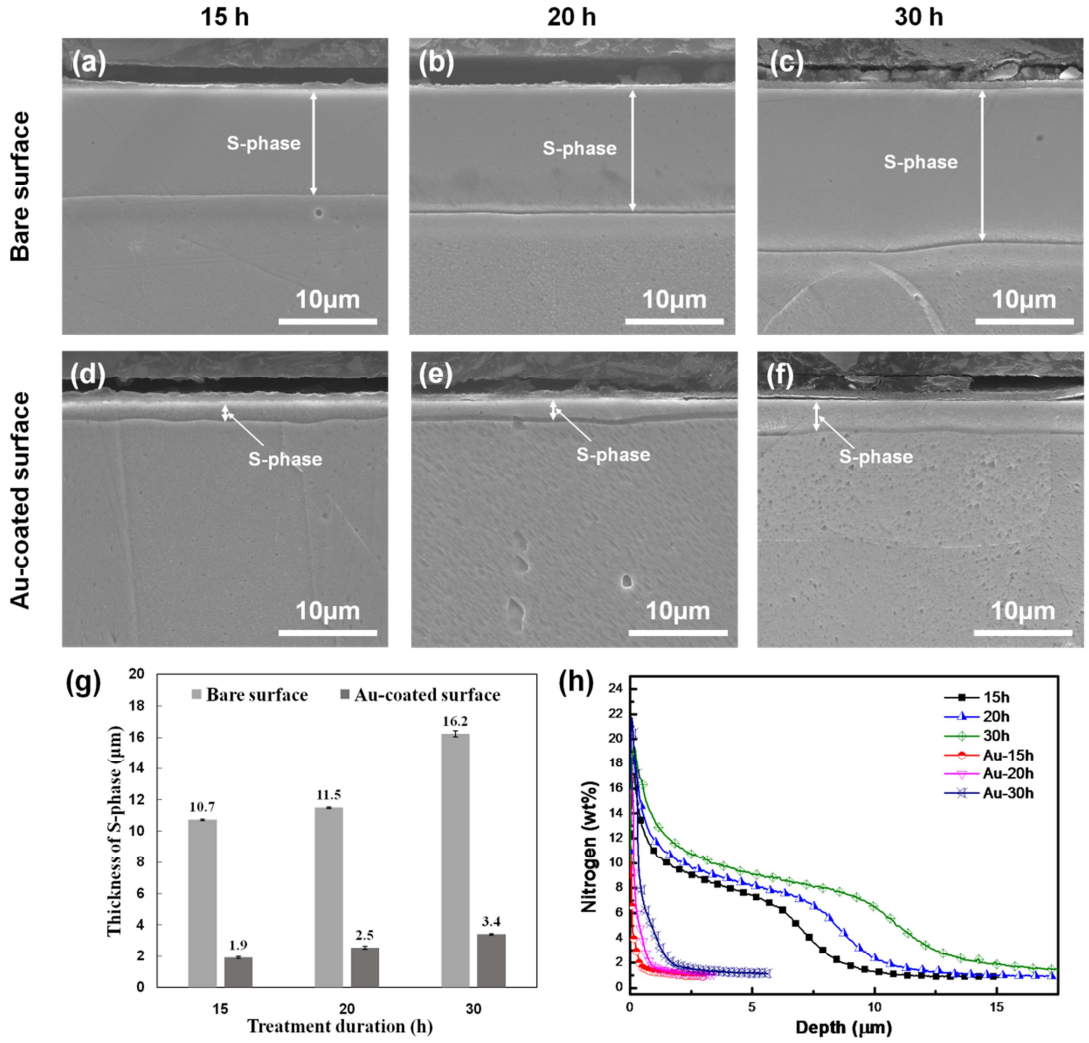

Figure 3 The low magnification cross-sectional SEM images of samples: (a) 15h, (b) 20h, (c) 30h, (d) Au-15h, (e) Au-20h, (f) Au-30h; (g) the S-phase layer thickness of samples; (h) the GDS nitrogen profiles of samples

The high magnification cross-sectional images of different surface are presented in Figure 4 (a-i). A thin layer (marked by white arrow) can be easily found on the very surface of each sample. This layer is the deposition layer, sputtered from the active screen and deposits onto the surface during ASPN treatment [3][27][28][13][29]. The thickness of deposition layers on different surfaces were measured and summarized in Figure 4 (j).

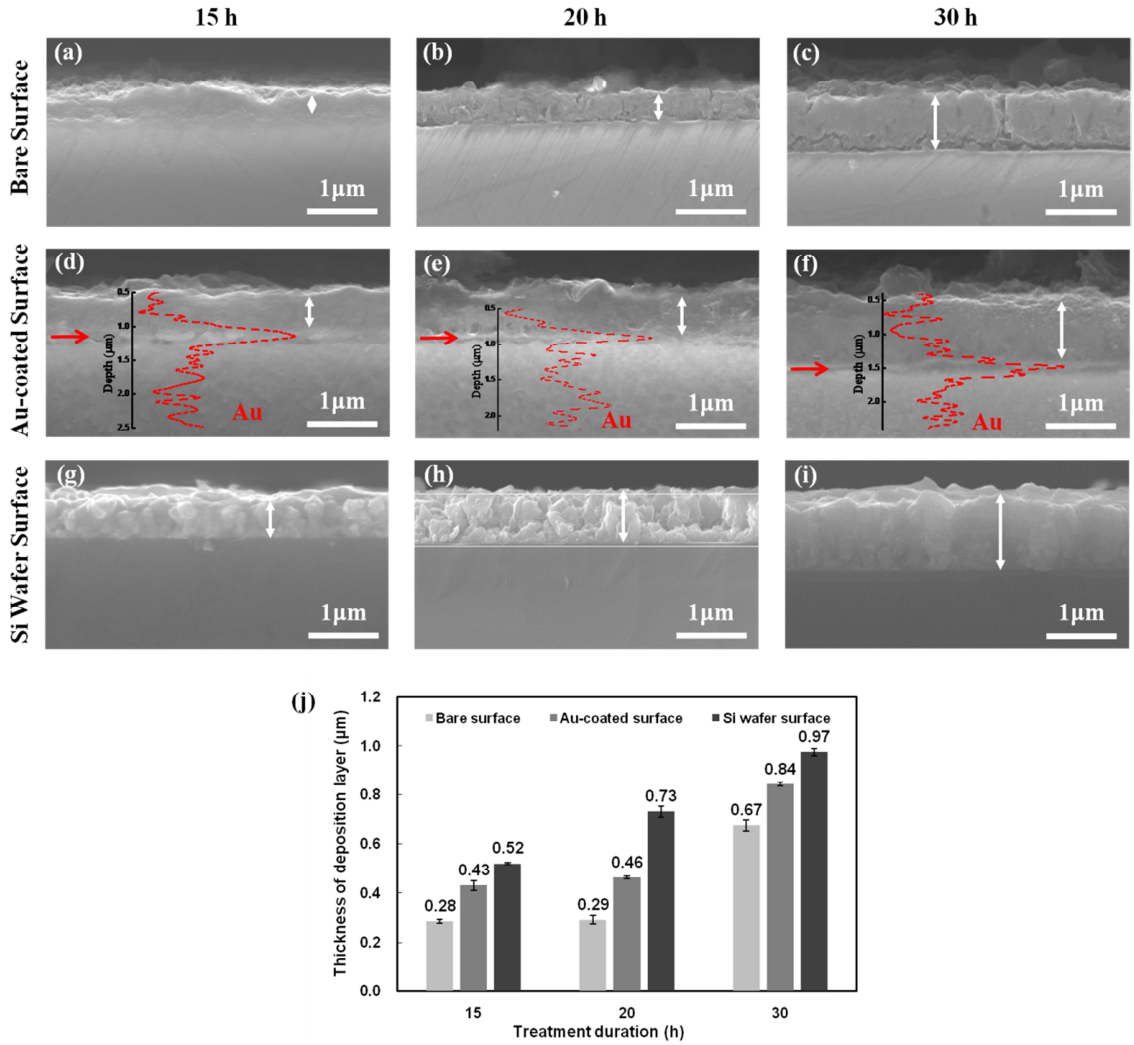

Figure 4 The high magnification cross-sectional SEM images of samples: (a) 15h, (b) 20h, (c) 30h, (d) Au-15h, (e) Au-20h, (f) Au-30h, (g) Si-15h, (h) Si-20h, (i) Si-30h; (j) the deposition layer thickness of samples

For the bare surfaces, the deposition layers are always the thinnest among three different surfaces under the same treatment duration. For the Au-coated surfaces, a complete and uniform layer (marked by red arrows), which sandwiched between the deposition layer and the S-phase layer, can be seen. The results of EDS line-scanning show that these layers are rich in Au, which confirms that these layers are Au coatings. For the Si wafer surfaces, the growth of deposition layer follows the “Stranski-Krastanov mode” (also called layer plus inland mode) [30] to form columnar grains on the surface (Figure 4 g-

i). For three different surfaces, the thickness of deposition layer increases with the increase of treatment duration. Under the same treatment duration, the deposition layer of the Si wafer surface is always the thickest, followed by that of the Au-coated surface and bare surface.

The results presented above clearly reveal that the bare surfaces, Au-coated surfaces and Si wafer surfaces exhibit completely different responds under the identical ASPN treatment condition. The bare surfaces have the thickest S-phase layer and the thinnest deposition layer; the Au-coated surfaces have much thinner S-phase layer and thicker deposition layer than that of the former; the Si wafer surfaces have no S-phase layer and the thickest deposition layer. The different nature of three surfaces results in those different responds and the schematic diagram of surface layer forming mechanisms of different surfaces are compared and presented in Figure 5. During the ASPN treatment, the nitrides, sputtered from the small active screen, deposits uniformly onto the three surfaces and builds up a nitrogen gradient [15]. For the bare surfaces, the active nitrogen atoms, releasing from the deposited nitrides, transfers into the substrate without any retardation by a diffusion controlled process and leads to the formation of S-phase. However, for the Au-coated samples, the Au-coating on the stainless steel surface could effectively retard but cannot completely block the nitrogen mass transfer from the deposition layer to the substrate. Therefore, small amount of nitrogen can still transfers through the Au-coating into the substrates and S-phase layers with much lower thickness and lower nitrogen content was formed (Figure 3 (g, h)). Because of the retardation of Au coating, more nitrogen was left within the deposition layer, leading to the higher nitrogen content than that of the bare surface. In addition, after ASPN treatment, a complete and uniform Au coating could still be found on top of the S-phase

layer, even after 30 hours treatment. This finding shows that no bombardment occurred during ASPN treatment, otherwise the Au coating would be damaged. For the Si wafer surfaces, because the solid solubility of nitrogen in Si is extremely low (9×10^{-6} at%) [22], all the deposited materials remain on the Si wafer surface without any nitrogen diffusion to the substrate, leading to the thickest layer and highest nitrogen content of the deposition layer among three surfaces.

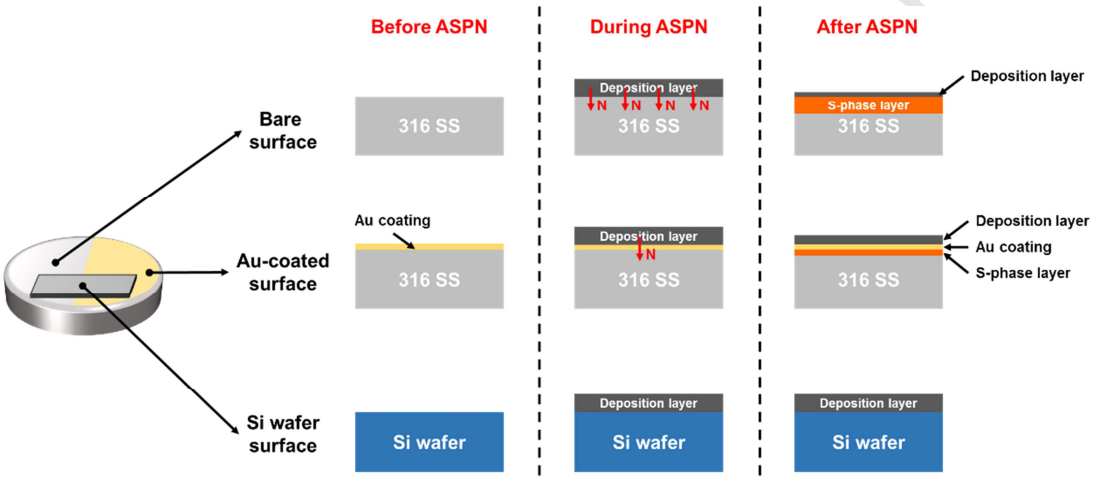

Figure 5 The schematic diagram of surface layer forming mechanisms of different surfaces

4. Conclusions

Based on the above results and discussions, one conclusion can be drawn that nitrogen mass transfer takes place between the deposition layer and the substrate by the decomposition of the nitrides in the deposition layer and the subsequent inward diffusion of active nitrogen atoms. This mass transfer leads to the reduction of layer thickness and nitrogen content of the surface deposition layer, and the formation of S-phase sublayer in the substrate.

Acknowledgement

The authors gratefully acknowledge the financial support from the EPSRC [grant number EP/J018252/1];the National Natural Science Foundation of China [grant numbers 51575267, 51322509]; the National Key Research and Development Program "Additive Manufacturing and Laser Manufacturing" [grant number 2016YFB1100101]; the Top-Notch Young Talents Program of China, the NSFC-DFG Sino-German Research Project [grant number GZ 1217]; the Key Research and Development Program of Jiangsu Provincial Department of Science and Technology of China [grant number BE2016181]; the 333 Project [grant number BRA2015368]; the Aeronautical Science Foundation of China [grant number 2015ZE52051]; the Program for New Century Excellent Talents in University [grant number NCET-13-0854]; the Fundamental Research Funds for the Central Universities [grant numbers NE2013103, NP2015206 and NZ2016108]; the Priority Academic Program Development of Jiangsu Higher Education Institutions. Kaijie Lin thanks the financial support from Natural Science Foundation of Jiangsu for Youths [grant number BK20170787] and the Research Start-up Fund of NUAA [grant number YAH16054].

Reference

[1] J. Georges, TC plasma nitriding, Heat Treat. Met. 28 (2001) 33–37.

[2] C.X. Li, J. Georges, X.Y. Li, Active screen plasma nitriding of austenitic stainless steel, Surf. Eng. 18 (2002) 453–457. doi:10.1179/026708402225006240.

[3] Y. Dong, X. Li, L. Tian, T. Bell, R.L. Sammons, H. Dong, Towards long-lasting antibacterial stainless steel surfaces by combining double glow plasma silvering with active screen plasma nitriding., Acta Biomater. 7 (2011) 447–57. doi:10.1016/j.actbio.2010.08.009.

[4] Y. Dong, X. Li, T. Bell, R. Sammons, H. Dong, Surface microstructure and antibacterial property of an active-screen plasma alloyed austenitic stainless steel surface with Cu and N., Biomed. Mater. 5 (2010) 54105. doi:10.1088/1748-6041/5/5/054105.

[5] Y. Dong, X. Li, R. Sammons, H. Dong, The generation of wear-resistant antimicrobial stainless steel surfaces by active screen plasma alloying with N and nanocrystalline Ag., J. Biomed. Mater. Res. B. Appl. Biomater. 93 (2010) 185–93. doi:10.1002/jbm.b.31573.

[6] X. Fu, R.L. Sammons, I. Bertóti, M.J. Jenkins, H. Dong, Active screen plasma surface modification of polycaprolactone to improve cell attachment., J. Biomed. Mater. Res. B. Appl. Biomater. 100 (2012) 314–20. doi:10.1002/jbm.b.31916.

[7] G. Kaklamani, J. Bowen, N. Mehrban, H. Dong, L.M. Grover, A. Stamboulis, Active screen plasma nitriding enhances cell attachment to polymer surfaces, Appl. Surf. Sci. 273 (2013) 787–798. doi:10.1016/j.apsusc.2013.03.001.

[8] X. Fu, M.J. Jenkins, G. Sun, I. Bertoti, H. Dong, Characterization of active screen plasma modified polyurethane surfaces, Surf. Coatings Technol. 206 (2012) 4799–4807. doi:10.1016/j.surfcoat.2012.04.051.

[9] K. Lin, X. Li, Y. Sun, X. Luo, H. Dong, Active screen plasma nitriding of 316 stainless steel for the application of bipolar plates in proton exchange membrane fuel cells, Int. J. Hydrogen Energy. 39 (2014) 21470–21479. doi:10.1016/j.ijhydene.2014.04.102.

[10] S. Du, K. Lin, S.K. Malladi, Y. Lu, S. Sun, Q. Xu, R. Steinberger-Wilckens, H. Dong, Plasma nitriding induced growth of Pt-nanowire arrays as high performance electrocatalysts for fuel cells., Sci. Rep. 4 (2014) 6439. doi:10.1038/srep06439.

[11] K. Lin, X. Li, L. Tian, H. Dong, Active screen plasma surface co-alloying of 316 austenitic stainless steel with both nitrogen and niobium for the application of bipolar plates in proton exchange membrane fuel cells, Int. J. Hydrogen Energy. 40 (2015) 10281–10292. doi:10.1016/j.ijhydene.2015.06.010.

[12] K. Lin, X. Li, L. Tian, H. Dong, Active screen plasma surface co-alloying treatments of 316 stainless steel with nitrogen and silver for fuel cell bipolar plates, Surf. Coatings Technol. 283 (2015) 122–128. doi:10.1016/j.surfcoat.2015.10.038.

[13] K. Lin, Y. Lu, S. Du, X. Li, H. Dong, The effect of active screen plasma treatment conditions on the growth and performance of Pt nanowire catalyst layer in DMFCs, Int. J. Hydrogen Energy. 41 (2016) 7622–7630. doi:10.1016/j.ijhydene.2016.02.008.

[14] K. Lin, X. Li, H. Dong, S. Du, Y. Lu, X. Ji, D. Gu, Surface modification of 316 stainless steel with platinum for the application of bipolar plates in high performance proton exchange membrane fuel cells, Int. J. Hydrogen Energy. 42 (2016) 2338–2348. doi:10.1016/j.ijhydene.2016.09.220.

[15] C.X. Li, T. Bell, H. Dong, A Study of Active Screen Plasma Nitriding, Surf. Eng. 18 (2002) 174–181. doi:10.1179/026708401225005250.

[16] C. Zhao, C.X. Li, H. Dong, T. Bell, Study on the active screen plasma nitriding and its nitriding mechanism, Surf. Coatings Technol. 201 (2006) 2320–2325. doi:10.1016/j.surfcoat.2006.03.045.

[17] C. Zhao, L.Y. Wang, L. Han, Active screen plasma nitriding of AISI 316L austenitic stainless steel at different potentials, Surf. Eng. 24 (2008) 188–192. doi:10.1179/174329408X271543.

[18] S. Corujeira Gallo, H. Dong, On the fundamental mechanisms of active screen plasma nitriding, Vacuum. 84 (2009) 321–325. doi:10.1016/j.vacuum.2009.07.002.

[19] P. Hubbard, S.J. Dowey, J.G. Partridge, E.D. Doyle, D.G. McCulloch, Investigation of nitrogen mass transfer within an industrial plasma nitriding

system II: Application of a biased screen, Surf. Coatings Technol. 204 (2010) 1151–1157. doi:10.1016/j.surfcoat.2009.08.030.

[20] P. Hubbard, J.G. Partridge, E.D. Doyle, D.G. McCulloch, M.B. Taylor, S.J. Dowey, Investigation of nitrogen mass transfer within an industrial plasma nitriding system I: The role of surface deposits, Surf. Coatings Technol. 204 (2010) 1145–1150. doi:10.1016/j.surfcoat.2009.08.029.

[21] L. B.X., Z. X., Grain growth induced by noble-metal films by N implantation, Phys. Status Solidi A. 124 (1991) K101-6.

[22] O.N. Carlson, The N-Si (Nitrogen-Silicon) system, Bull. Alloy Phase Diagrams. 11 (1990) 569–573. doi:10.1007/BF02841719.

[23] H. Dong, P.Y. Qi, X.Y. Li, R.J. Llewellyn, Improving the erosion-corrosion resistance of AISI 316 austenitic stainless steel by low-temperature plasma surface alloying with N and C, Mater. Sci. Eng. A. 431 (2006) 137–145. doi:10.1016/j.msea.2006.05.122.

[24] S. Corujeira Gallo, H. Dong, EBSD and AFM observations of the microstructural changes induced by low temperature plasma carburising on AISI 316, Appl. Surf. Sci. 258 (2011) 608–613. doi:10.1016/j.apsusc.2011.06.158.

[25] S. Corujeira Gallo, H. Dong, New insights into the mechanism of low-temperature active-screen plasma nitriding of austenitic stainless steel, Scr. Mater. 67 (2012) 89–91. doi:10.1016/j.scriptamat.2012.03.028.

[26] H. Dong, S-phase surface engineering of Fe-Cr, Co-Cr and Ni-Cr alloys, Int. Mater. Rev. 55 (2010) 65–98. doi:10.1179/095066009X12572530170589.

[27] S. Corujeira Gallo, H. Dong, Study of active screen plasma processing conditions for carburising and nitriding austenitic stainless steel, Surf. Coatings Technol. 203 (2009) 3669–3675. doi:10.1016/j.surfcoat.2009.05.045.

[28] A. Nishimoto, K. Nagatsuka, R. Narita, H. Nii, K. Akamatsu, Effect of the distance between screen and sample on active screen plasma nitriding properties, Surf. Coatings Technol. 205 (2010) S365–S368. doi:10.1016/j.surfcoat.2010.08.034.

[29] C.X. Li, Active screen plasma nitriding – an overview, Surf. Eng. 26 (2010) 135–141. doi:10.1179/174329409X439032.

[30] J.A. Venables, Introduction to Surface and Thin Film Processes, Cambridge University Press, 2000. http://dx.doi.org/10.1017/CBO9780511755651.

Figure Captions

Figure 1 Schematic diagram of active screen plasma nitriding treatments

Figure 2 The surface morphology SEM images of different surfaces: (a) Bare-15h, (b) Bare-20h, (c) Bare-30h, (d) Au-15h, (e) Au-20h, (f) Au-30h,(g) Si-15h, (h) Si-20h, (i) Si-30h; (j) the XRD patterns of Si-30h sample; (k) the nitrogen contents of bare surfaces, Au-coated surfaces and Si surfaces after different treatment durations

Figure 3 The low magnification cross-sectional SEM images of samples: (a) 15h, (b) 20h, (c) 30h, (d) Au-15h, (e) Au-20h, (f) Au-30h; (g) the S-phase layer thickness of samples; (h) the GDS nitrogen profiles of samples

Figure 4 The high magnification cross-sectional SEM images of samples: (a) 15h, (b) 20h, (c) 30h, (d) Au-15h, (e) Au-20h, (f) Au-30h, (g) Si-15h, (h) Si-20h, (i) Si-30h; (j) the deposition layer thickness of samples

Figure 5 The schematic diagram of surface layer forming mechanisms of different surfaces

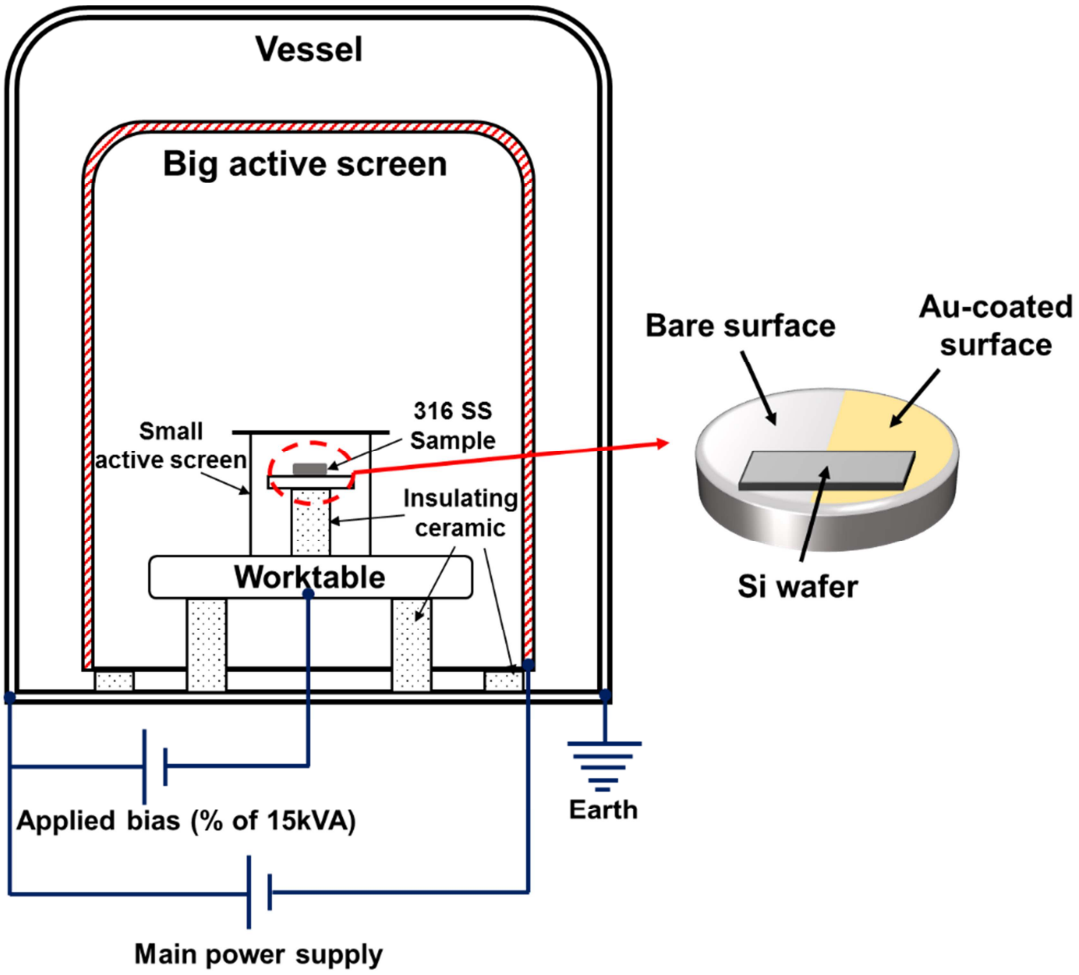

Figure 1 Schematic diagram of active screen plasma nitriding treatments

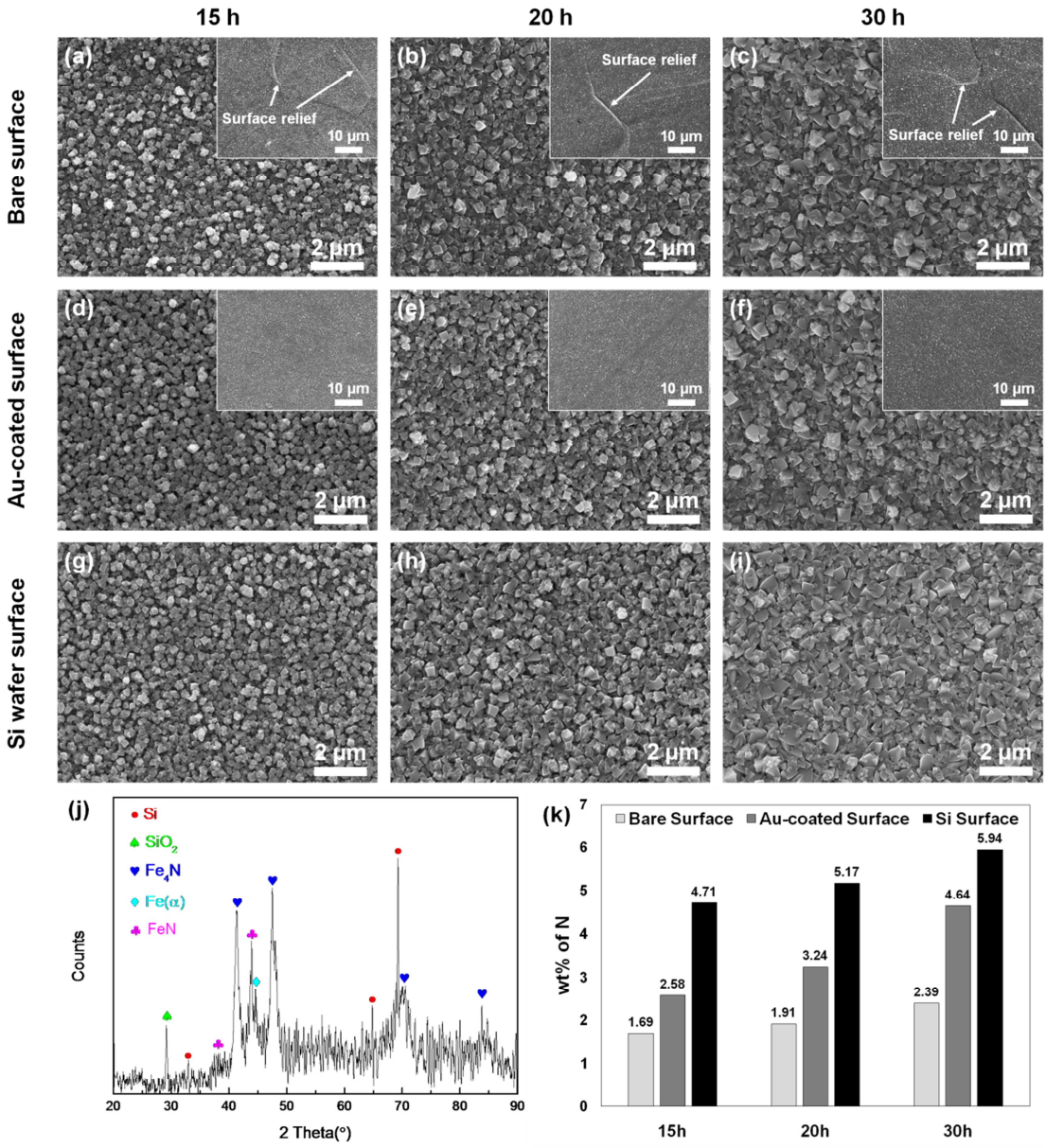

Figure 2 The surface morphology SEM images of different surfaces: (a) Bare-15h, (b) Bare-20h, (c) Bare-30h, (d) Au-15h, (e) Au-20h, (f) Au-30h,(g) Si-15h, (h) Si-20h, (i) Si-30h; (j) the XRD patterns of Si-30h sample; (k) the nitrogen contents of bare surfaces, Au-coated surfaces and Si surfaces after different treatment durations

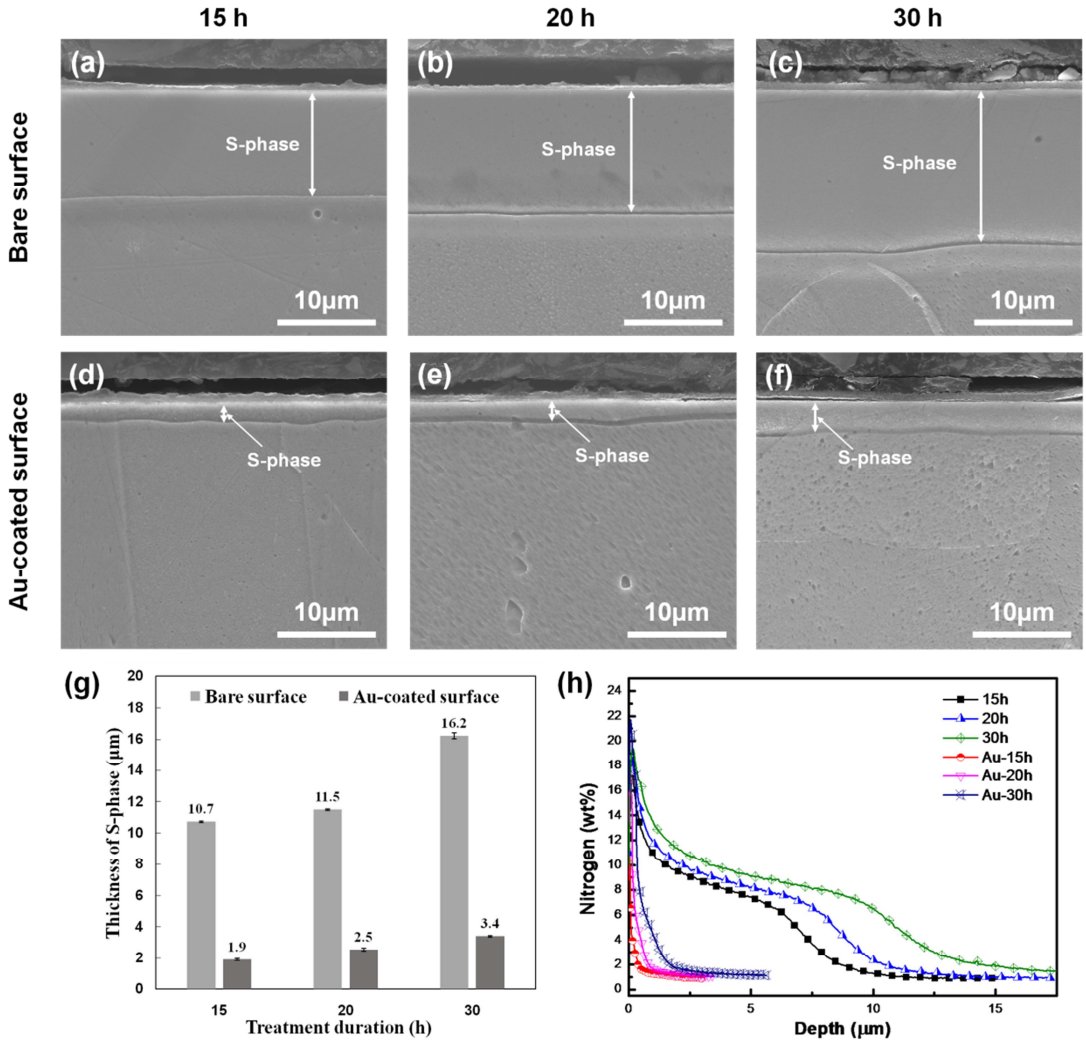

Figure 3 The low magnification cross-sectional SEM images of samples: (a) 15h, (b) 20h, (c) 30h, (d) Au-15h, (e) Au-20h, (f) Au-30h; (g) the S-phase layer thickness of samples; (h) the GDS nitrogen profiles of samples

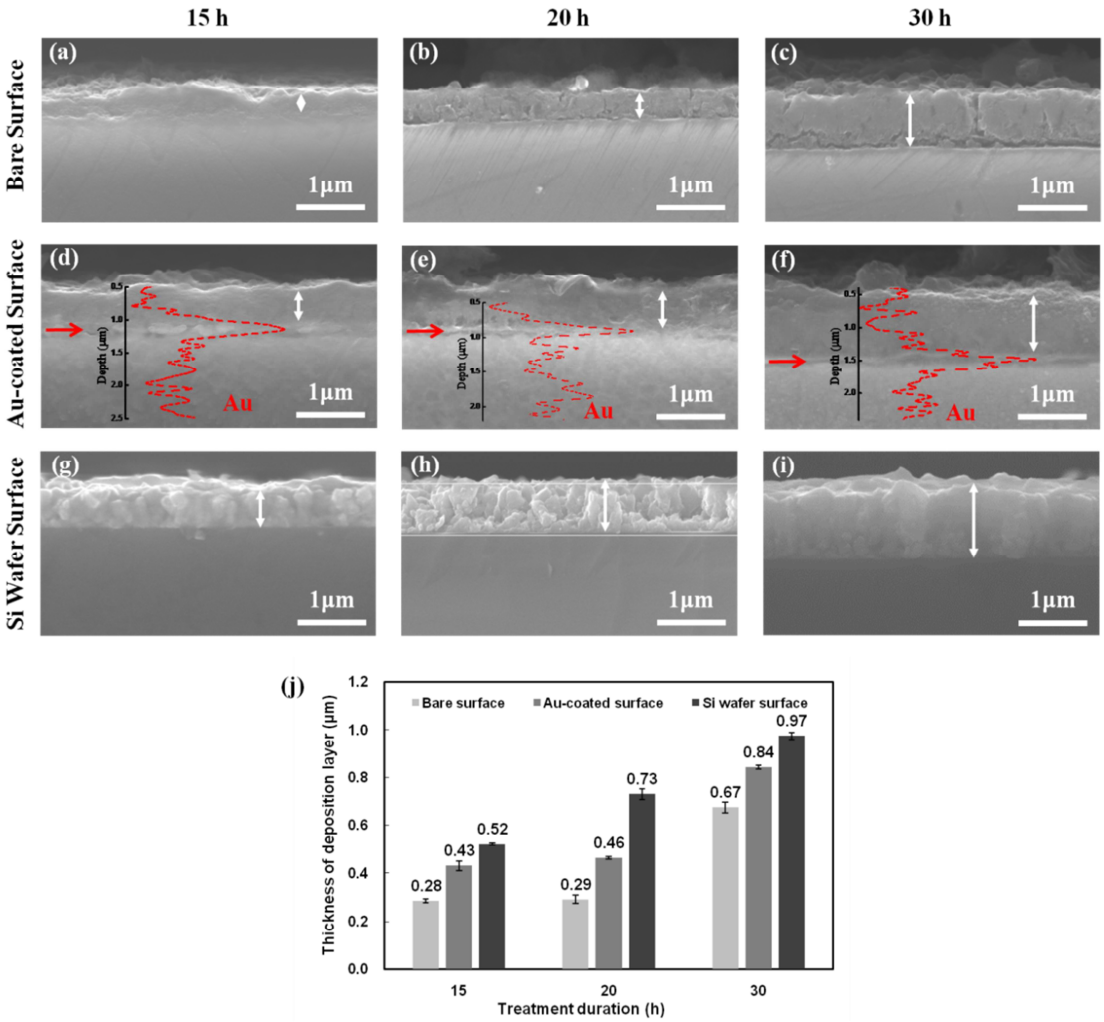

Figure 4 The high magnification cross-sectional SEM images of samples: (a) 15h, (b) 20h, (c) 30h, (d) Au-15h, (e) Au-20h, (f) Au-30h, (g) Si-15h, (h) Si-20h, (i) Si-30h; (j) the deposition layer thickness of samples

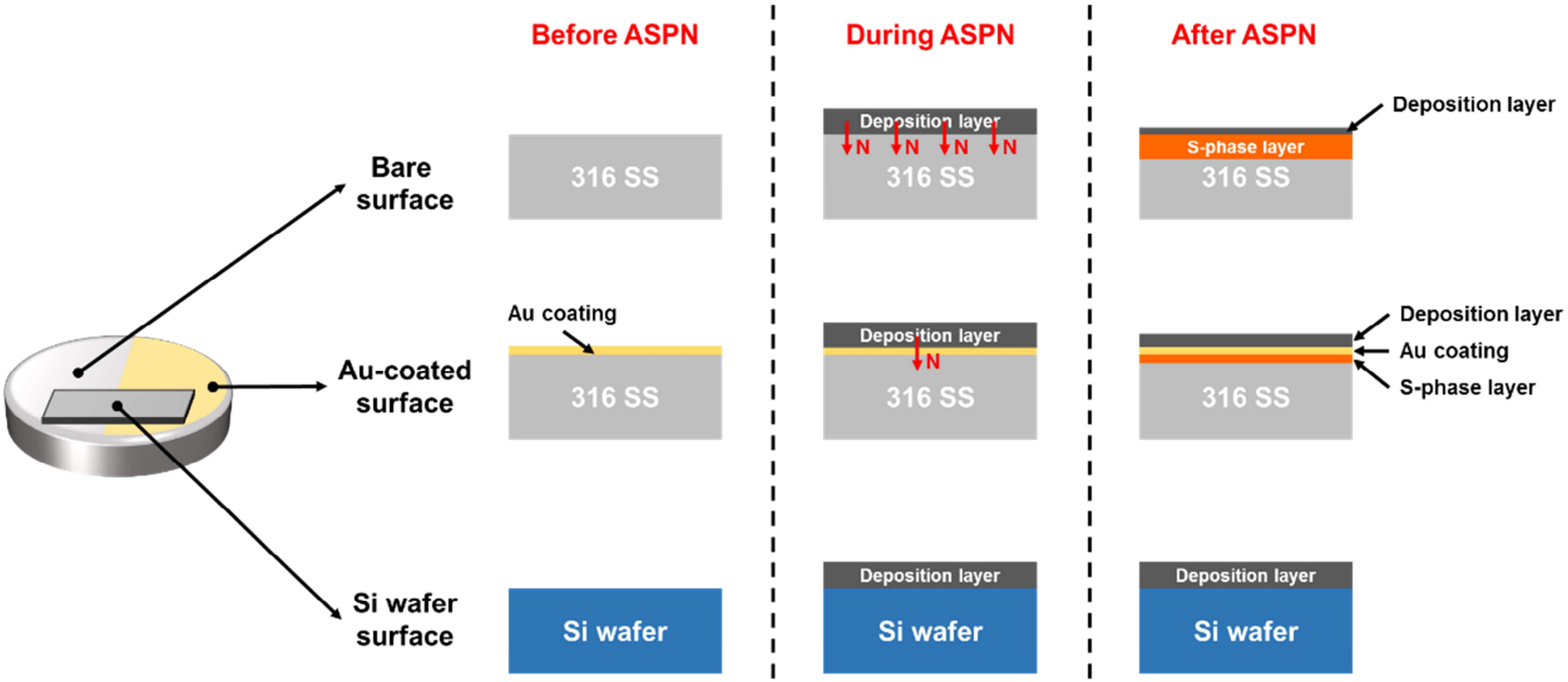

Figure 5 The schematic diagram of surface layer forming mechanisms of different surfaces

- Three different surfaces were active-screen-plasma-nitrided simultaneously.
- The surface layer formation of different surfaces was investigated and compared.
- The nitrogen transfer between the deposition layer and the substrate was confirmed.